Journal of the Meteorological Society of Japan, Vol. 75, No. 2, pp. 513–527, 1997

An Analysis of Summer Rain Showers over Central Japan and its Relation with the Thermally Induced Circulation

By **Tsuneo Kuwagata**

Tohoku National Agricultural Experiment Station, Morioka, 020-01 Japan

(Manuscript received 9 May 1996, in revised form 24 December 1996)

Abstract

The summer rain shower which develop in central Japan under otherwise fair-weather conditions during the summer of 1985 were investigated, making use of routine observational data from weather stations. According to the statistical analysis, the diurnal cycle of precipitation exhibited a distinct peak around 1800 LST, while little rainfall occurred from 0000 to 1200 LST. This distinct peak was associated with the summer rain shower developed over the heated land surface during the afternoon. The rain shower activity increased as the atmospheric static stability for dry (or moist) convection decreased, under conditions that the atmospheric precipitable water exceeded 40 mm. The rain shower was concentrated in the mountainous regions which consist of several mountain ranges having the horizontal scale of about 100 km. The areas where the rain shower was concentrated largely did not move with time. The degree of spatial concentration of the rain showers however was weaker under higher activity conditions of the rain showers.

A thermally induced local circulation developed over central Japan during the daytime under fair weather and weak synoptic wind conditions from the spring to summer seasons. This circulation was strongly dependent on the topography, and converged in the mountainous regions. According to the previous study, the daytime thermally induced circulation contributes to an increase in the water vapor content over the mountainous regions through the moist air advection from the plain and basin regions, and the greatest amounts of water vapor are accumulated over the mountainous regions in the late afternoon when the horizontal scale of topography is close to 100 km. Specific humidity measured in the mountainous area displayed an afternoon maximum, exceeding that at the basin bottom in the afternoon. The increase in water vapor over the mountainous regions is expected to contribute to the development of cumulus clouds, which was confirmed by decreased sunshine duration during the late afternoon over the mountainous regions. These results suggest that summer rain showers are triggered over the mountainous regions by the thermally-induced local circulation.

1. Introduction

The so-called heat thunderstorm, which is a convective rain shower resulting from the development of cumulus and cumulonimbus clouds over a heated ground surface during the daytime, is one of several typical meteorological phenomena that occur in central Japan during the summer. This type of thunderstorm frequently forms over mountainous areas during the afternoon of an otherwise sunny day, and occasionally causes severe rainfall and lightning. Statistical analyses of daily precipitation cycles using routine observational data reveal that a peak is formed in the evening rainfall due to the rain showers occurring over the inland area of central Japan during the summer (Fujibe, 1988; Tatehira and Hoshina, 1993; Oki and Musiake, 1994).

On the other hand, a thermally-induced local circulation can develop under fair-weather and weak synoptic wind conditions over the spring to summer seasons (Shimizu, 1964; Suzuki, 1991; Kuwagata *et al.*, 1990). The thermally induced circulation results from a horizontally non-uniform heat source, and is strongly affected by the topography. Several studies have focused on the relationship between the thermally induced circulation and the summer rain shower. Udagawa (1966; 1968) pointed out that the thermally induced circulation may act as a trigger for summer thunderstorms over the inland area of central Japan. A statistical analysis, using routine observational data, revealed that the sunshine duration decreased at the weather stations over the mountainous area of central Japan in the afternoon of otherwise fair-weather conditions due to the development of clouds (Kimura, 1994). Kuwagata and

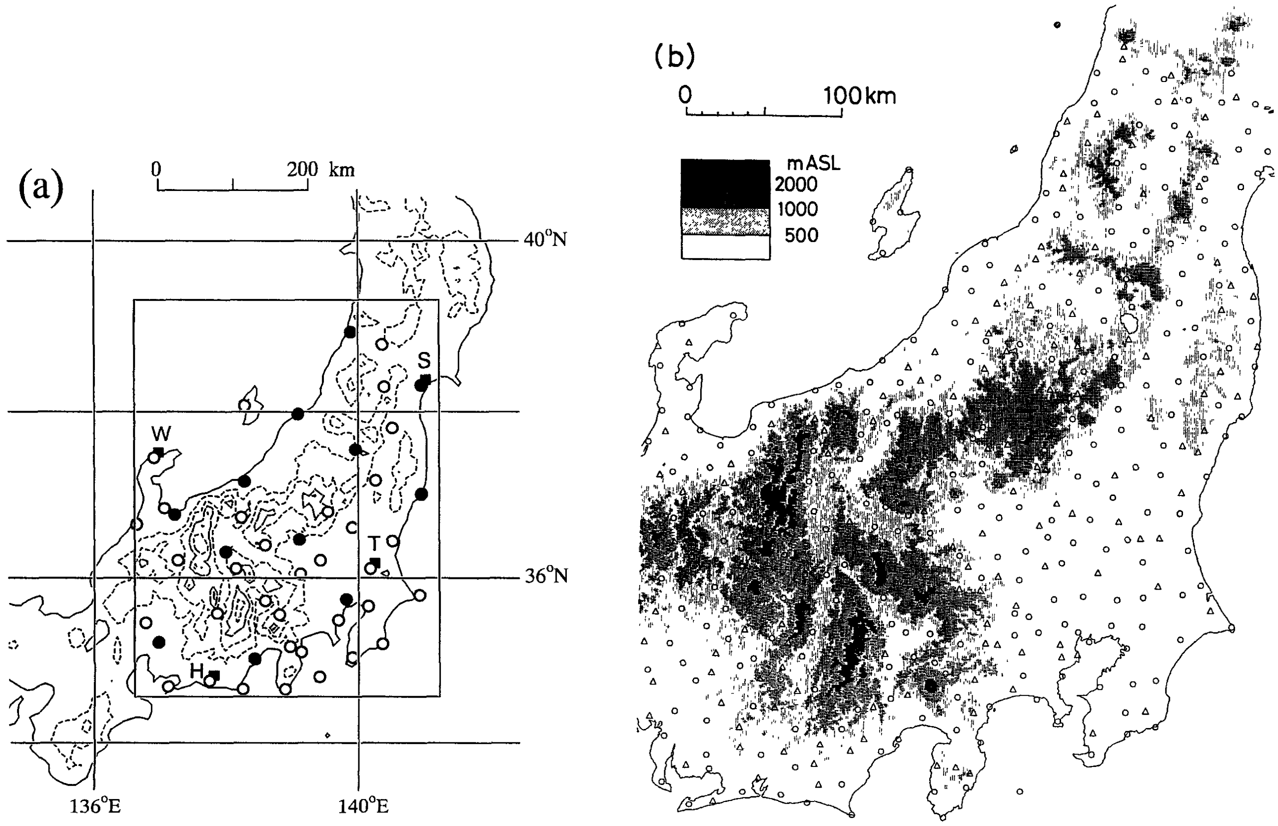

Fig. 1. Map showing the area of central Japan. (a) Meteorological stations are indicated by circles (solid circles denote the representative meteorological stations), and aerological stations by solid squares (S: Sendai, W: Wajima, T: Tateno, H: Hamamatsu). The broken contour lines indicate elevation for every 500 m above MSL. (b) The analysis area represented by the rectangular region given in (a). The various degrees of shading indicate height above mean sea level (m MSL). AMeDAS stations are indicated by open circles and automated rain stations by open triangles.

Kimura (1995; 1997) further showed that the thermally induced cross-valley circulation in a deep valley can result in the formation of cumulus clouds over the mountain ridges during the afternoon.

In the present study, both the characteristics of the summer rain shower and the contribution from the thermally induced local circulation to the development of rain showers in central Japan are investigated using routine observational data from weather stations in the summer. The thermally induced circulation can also develop under fair-weather and weak synoptic wind conditions during the spring season (as will be defined in the present study), when the daytime sensible heat flux is at its strongest of the year. However, few rain showers occur under such conditions in the spring. In order to examine the difference in the thermally induced circulation over central Japan between spring and summer, springtime weather data are also analyzed.

2. Data

Figure 1 shows a map of central Japan. The region analyzed (the area identified by the rectangle in Fig. 1a) consists of many mountain ranges, basins and plains, and covers an area of 123,600 km^2. The horizontal scale of topography, which corresponds to the distance between adjacent mountain ranges, the length of each mountain range, or the widths of each basin and plain, is about 100 km in central Japan (ranging from 50 km to 150 km for each topography). The vertical scale of each mountain range exceeds 2 km. There are 46 meteorological stations, 281 Automated Meteorological Data Acquisition System (AMeDAS) stations, and 169 automated rain stations in this region, along with 4 aerological stations. The main data source in the present analysis consists of the AMeDAS and Automated rain stations.

In order to analyze the characteristics of summer rain shower and the contribution of the thermally-induced local circulation to the development of rain showers, the summer season of 1985 was selected. The summer of 1985 is suitable for the present analysis, since a period of hot weather continued for a long time. The 37 sunny summer days during 1985, which were days of fair weather having favorable conditions for the development of a rain shower, were selected by the following procedure:

(1) First, the 1985 summer season was defined as the 50-day period from 19 July to 6 September. During this period, Japan was mostly under the influence of a Pacific anticyclone.

(2) The days when part of central Japan was covered by clouds of a tropical cyclone or synoptic frontal zone were excluded from the analysis. The cloudy areas associated with tropical cyclones and synoptic frontal zones were identified from weather charts, the visible and infrared images of the Geostationary Meteorological Satellite (GMS), and the rainfall and sunshine data from AMeDAS stations. The excluded days were 5–12, 20, 30–31 August, and 1–2 September, resulting in 37 days of sunny summer weather being selected from the 50-days of the 1985 summer season.

The daily mean wind speed at 700 hPa averaged for the 4 aerological stations ranged from 3.4 to 9.9 ms^{-1} for the 37 summer days (6.0 ms^{-1} averaged over the 37 days), and a westerly wind was dominant at 700 hPa during most of the period. That is, the upper-level synoptic wind was weak during this period. On the other hand, the daily sunshine duration averaged for the 281 AMeDAS stations ranged from 6.8 to 11.3 h for the 37 summer days (9.5 h averaged over the 37 days).

In order to examine the difference in the thermally induced local circulation over central Japan between spring and summer, fair-weather days during the spring (46 days) with weak synoptic winds are also analyzed. The 46 sunny spring days were selected from the spring seasons (from 25 April to 15 June) during 1980 to 1986, which satisfy the following criteria:

(1) For the 12 representative meteorological stations (see Fig. 1), there must have been more than 9 sites where the daily sunshine duration N_d was ≥ 10 h, and no sites with $N_d < 7$ h.

(2) For the 12 representative meteorological stations, there must have been more than 9 sites where no rainfall occurred, and no sites with the daily precipitation amount $P > 0.5$ mm.

(3) The absolute value of the temperature change at 700 hPa from 0900 to 2100 Japan Standard Time (JST) $|\Delta T_{700\ \mathrm{hPa}}|_{09\text{–}21\ \mathrm{JST}}$, averaged for the 4 aerological stations, must have been $< 3°$C.

(4) The upper-level (800 hPa) wind speeds at both 0900 and 1500 JST $V_{800\ \mathrm{hPa}}$ must have been $< 10\mathrm{ms}^{-1}$ at 3 of the 4 aerological stations at least.

Items (1)–(4) correspond to the conditions for calm fair weather with weak synoptic winds, being suitable for the development of the typical thermally induced circulation over central Japan.

3. Analysis of rainfall

In this section, the summer rain showers are analyzed using hourly precipitation data from the AMeDAS and automated rain stations, a total of 450 sites.

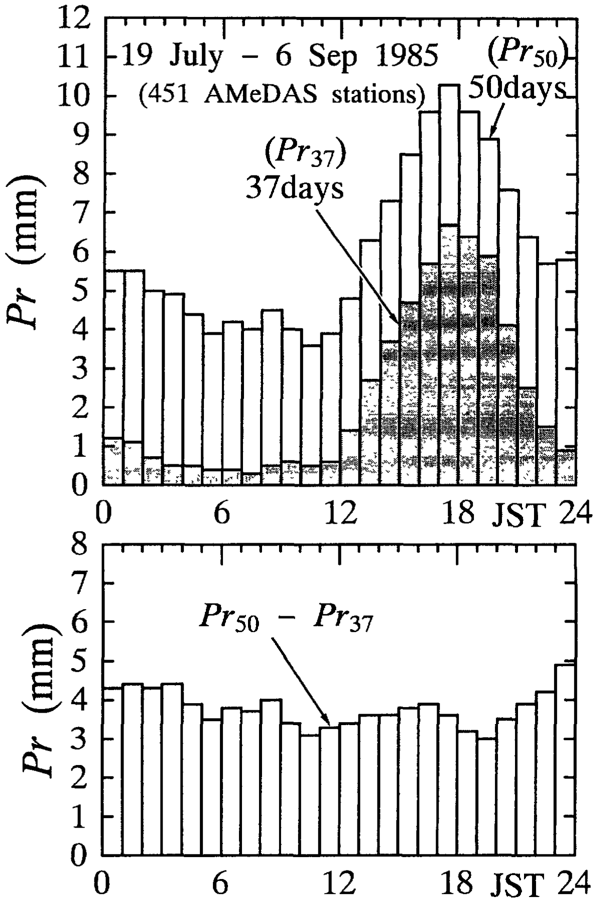

Fig. 2. The daily variation of hourly rainfall averaged for the 450 stations. The values of total rainfall for the 1985 summer season (50 days from 19 July to 6 September) Pr_{50} are indicated by the tops of the open bars, and those for the 37 days of summer Pr_{37} by the tops of the shaded bars (top panel). The value of $Pr_{50} - Pr_{37}$ is also shown (bottom panel).

3.1 Daily variation

Figure 2 shows the daily variation of the hourly rainfall averaged for the 450 stations. Here, the total rainfall amounts for the 1985 summer season (50 days from 19 July to 6 September) Pr_{50} are indicated by the top of the open bars (top panel), and the rainfall for the 37 summer days Pr_{37} by the top of the shaded bars. The values of $Pr_{50} - Pr_{37}$ are also shown in Fig. 2 (bottom panel). For the 50 days during the summer season, a distinct peak in the evening rainfall can be seen around 1800 JST. For the 37 sunny days, although a distinct peak in evening rainfall around 1800 JST still exists, little rainfall occurs from 0000 to 1200 JST. The total rainfall for the 37 days reaches 53.5 mm.

A rainfall event at each site is defined as one continuous rainy period having over 1 mm rainfall. It is possible to have 2–3 rainfall events for a given day at each site. The duration of rainfall events occurring at each site for the 37 days was only 1.8 h on average, and over 90 % of rainfall events had a duration of less than 3 h. That is, most of rainfall events for the 37 sunny summer days can be considered as rain showers associated with the development of cumulus and cumulonimbus clouds during the afternoon. Figure 2 also shows little daily variation of rainfall due to summer tropical cyclones and synoptic fronts for the summer in 1985.

3.2 Variation of daily rainy activity

The development of a rain shower should strongly depend on the vertical thermal structure of the lower troposphere. Therefore, the upper air data at the aerological stations were used to investigate variations in the daily activity of the rain showers.

Figure 3a shows the relationship between the static stability for dry convection $\Delta\theta$ and the rainfall amount from 1200 to 2400 JST $Pr_{12\text{–}24\ \mathrm{JST}}$, averaged for the 450 stations for each of the 37 days of sunny summer weather. Here, $\Delta\theta\,(=\overline{\theta}_{sfc-850\ \mathrm{hPa}}-\theta_{500\ \mathrm{hPa}})$ represents the average dry static stability for the 3 aerological stations (Wajima, Tateno, and Hamamatsu, see Fig. 1a) at 0900 JST, where $\overline{\theta}_{sfc-850\ \mathrm{hPa}}$ is the mean potential temperature from the surface to 850 hPa, and $\theta_{500\ \mathrm{hPa}}$ the potential temperature at 500 hPa. The open circles indicate the results of data for atmospheric precipitable water w having values < 40 mm, while the solid circles $w \geq 40$ mm at 0900 JST, averaged for the 3 aerological stations. The value of $w = 40$ mm also corresponds to the mean value of w for the 37 days. The static stability for dry convection decreases as the value of $\Delta\theta$ increases. According to Fig. 3a, rainfall amounts $Pr_{12\text{–}24\ \mathrm{JST}}$ increase as the static stability for dry convection decreases under conditions of $w \geq 40$ mm.

Figure 3b demonstrates the relationship between the static stability for moist convection and the rainfall amount $Pr_{12\text{–}24\ \mathrm{JST}}$ averaged for the 450 stations for each of the 37 days. In this figure, the static stability for moist convection is represented as $\overline{\theta}_{e,sfc-850\ \mathrm{hPa}}-\theta^*_{e,500\ \mathrm{hPa}}$, averaged for the 3 aerological stations at 0900 JST, where $\overline{\theta}_{e,sfc-850\ \mathrm{hPa}}$ is the mean equivalent potential temperature from the surface to 850 hPa, and $\theta^*_{e,500\ \mathrm{hPa}}$ the pseudo-equivalent potential temperature at 500 hPa. The rainfall amounts $Pr_{12\text{–}24\ \mathrm{JST}}$ increase as the moist static stability decreases under conditions of $w \geq 40$ mm, being similar to the result for dry static stability (Fig. 3a). It should be noted that the dependence on the value of w is somewhat weaker than that for the dry static stability since the moist static stability decreases with increasing the water vapor content in the lower troposphere.

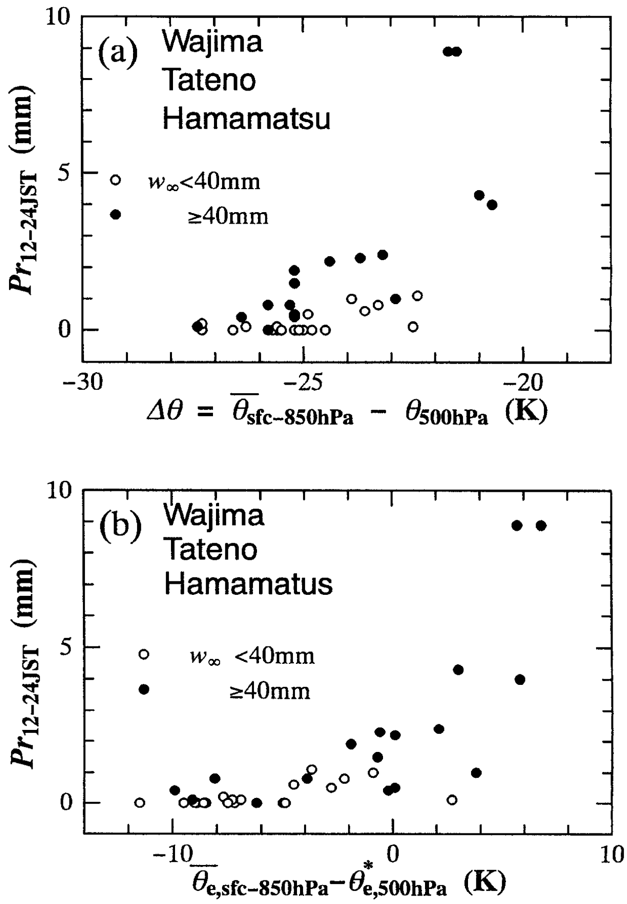

Fig. 3. (a) The relationships between the static stability for dry convection $\Delta\theta$ and the rainfall amount $Pr_{12\text{–}24\ \mathrm{JST}}$ from 1200 to 2400 JST averaged for 450 stations for each day of the 37 summer days. Here, $\Delta\theta\,(=\overline{\theta}_{sfc-850\ \mathrm{hPa}}-\theta_{500\ \mathrm{hPa}})$ is the average for the 3 aerological stations (Wajima, Tateno, and Hamamatsu) at 0900 JST, where $\overline{\theta}_{sfc-850\ \mathrm{hPa}}$ is the mean potential temperature from the surface to 850 hPa, and $\theta_{500\ \mathrm{hPa}}$ the potential temperature at 500 hPa. The open circles correspond to the data for atmospheric precipitable water $w < 40$ mm, while the solid circles for $w \geq 40$ mm at 0900 JST, averaged for the 3 aerological stations. (b) As in Fig. 3a, except for the static stability for moist convection. The static stability for moist convection is represented by $\overline{\theta}_{e,sfc-850\ \mathrm{hPa}}-\theta^*_{e,500\ \mathrm{hPa}}$ averaged for the 3 aerological stations at 0900 JST, where $\overline{\theta}_{e,sfc-850\ \mathrm{hPa}}$ is the mean equivalent potential temperature from the surface to 850 hPa, and $\theta^*_{e,500\ \mathrm{hPa}}$ is the pseudo-equivalent potential temperature at 500 hPa.

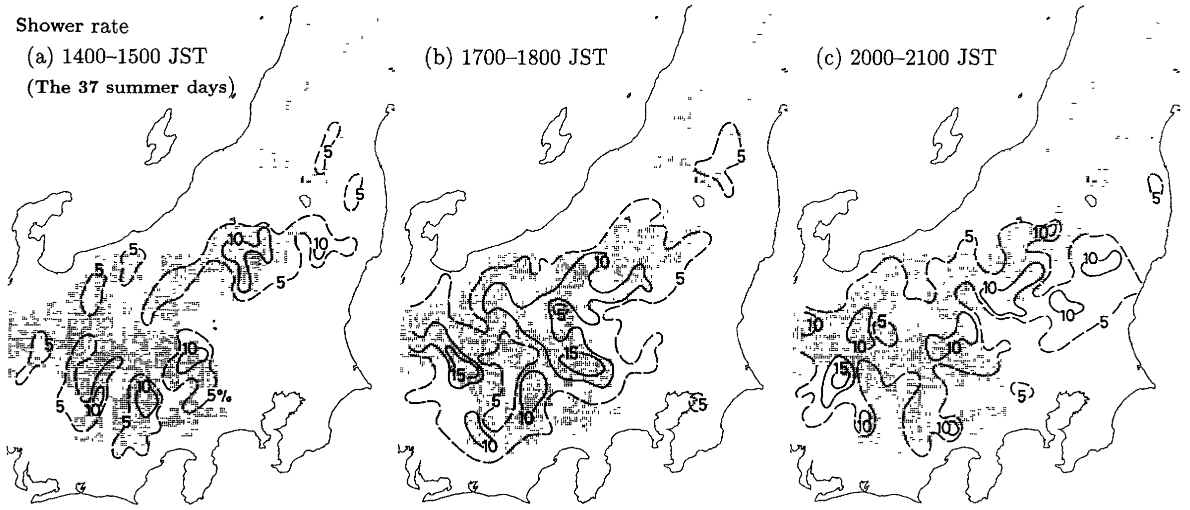

Fig. 4. The distribution of shower rate for three periods of the 37 summer days, (a) the 1st period (1400 to 1500 JST), (b) the 2nd period (1700 to 1800 JST) ,and (c) the 3rd period (2000 to 2100 JST). Here, the shower rate at each site is defined as $100 \times n/n_{\max}$ (%), where n is the number of days having over 1 mm rainfall during a given period, and $n_{\max} = 37$ (days). Regions of elevation higher than 800 m MSL, averaged over 10 km $\times$ 10 km grid boxes, are stippled.

From the results above, we can conclude that rain shower activity becomes greater when the precipitable water exceeds 40 mm, and that under such conditions, rainfall amounts due to rain showers increase as the static stability of atmosphere for dry (or moist) convection decreases.

3.3 Spatial distribution

The spatial distribution of rain shower activity is analyzed, making use of the hourly precipitation data from the 450 stations. Figure 4 shows the distribution of shower rate for three periods, the first period (1400 to 1500 JST), the second period (1700 to 1800 JST), and the third period (2000 to 2100 JST). Here, the shower rate at each site is defined as $100 \times n/n_{\max}$ (%), where n is the number of days having over 1 mm rainfall during a given period, and $n_{\max} = 37$ (days). The active rainy areas, which are the areas having greater shower rates, are concentrated in the mountainous regions for the 1st and 2nd periods, where the 1st period corresponds to the developing stage of the rain showers, and the 2nd period to the developed stage. For the 3rd period, the decaying stage of the rain showers, the active rainy areas still remain over the mountainous regions, whereas part of the active rainy areas move to north of the Kanto Plain (the location of the Kanto Plain is indicated in Fig. 12). The active rainy area north of the Kanto Plain must be mainly caused by the movement of rain shower clouds from the mountainous regions due to upper-level westerly wind.

The active rainy areas over the mountainous regions are almost stationary during the afternoon except for the north of the Kanto Plain, in spite of the upper-level westerly wind. Hereafter, the rain data from 1200 to 2400 JST are analyzed in order to clarify the spatial distribution of rain shower activity. Figure 5a shows the frequency distribution of rainfall events that occurred from 1200 to 2400 JST for the 37 summer days. The rainfall events are concentrated in the mountainous regions. That is, the frequencies of rainfall events are fewer in the plain and basin areas, such as the Kanto Plain, the Kofu Basin, and the Ina Valley (see Fig. 12), while those are greater over the mountain ranges surrounding these plain and basin areas. Only north of the Kanto Plain, greater frequencies of the rainfall events spread over the southeast side of the mountains, resulting from the movement of the active rainy area with time (see Fig. 4). Figure 5b, on the other hand, shows the distribution of total rainfall amounts from 1200 to 2400 JST for the 37 days. Areas of heavy total rainfall amounts are also concentrated in the mountainous regions, although the horizontal extension of the rainfall amounts is somewhat greater than for the frequency distribution of rainfall events.

Next, the 37 summer days are divide into two groups according to the rainfall amount on each day $Pr_{12\text{–}24\ \mathrm{JST}}$ averaged for all stations. Here, the active rainy case (4 days, 20–22 June, and 6 September) corresponds to the conditions of $Pr_{12\text{–}24\ \mathrm{JST}} \geq 4$ mm, and the normal rainy case (33 days) to the conditions of $Pr_{12\text{–}24\ \mathrm{JST}} < 4$ mm. The spatial distribution of rain shower activity is also analyzed for each case. Figure 6 shows the frequency distribution of afternoon rainfall events (1200 to 2400 JST) and the distribution of total afternoon rainfall amounts for the active rainy case, while Fig. 7 shows those for

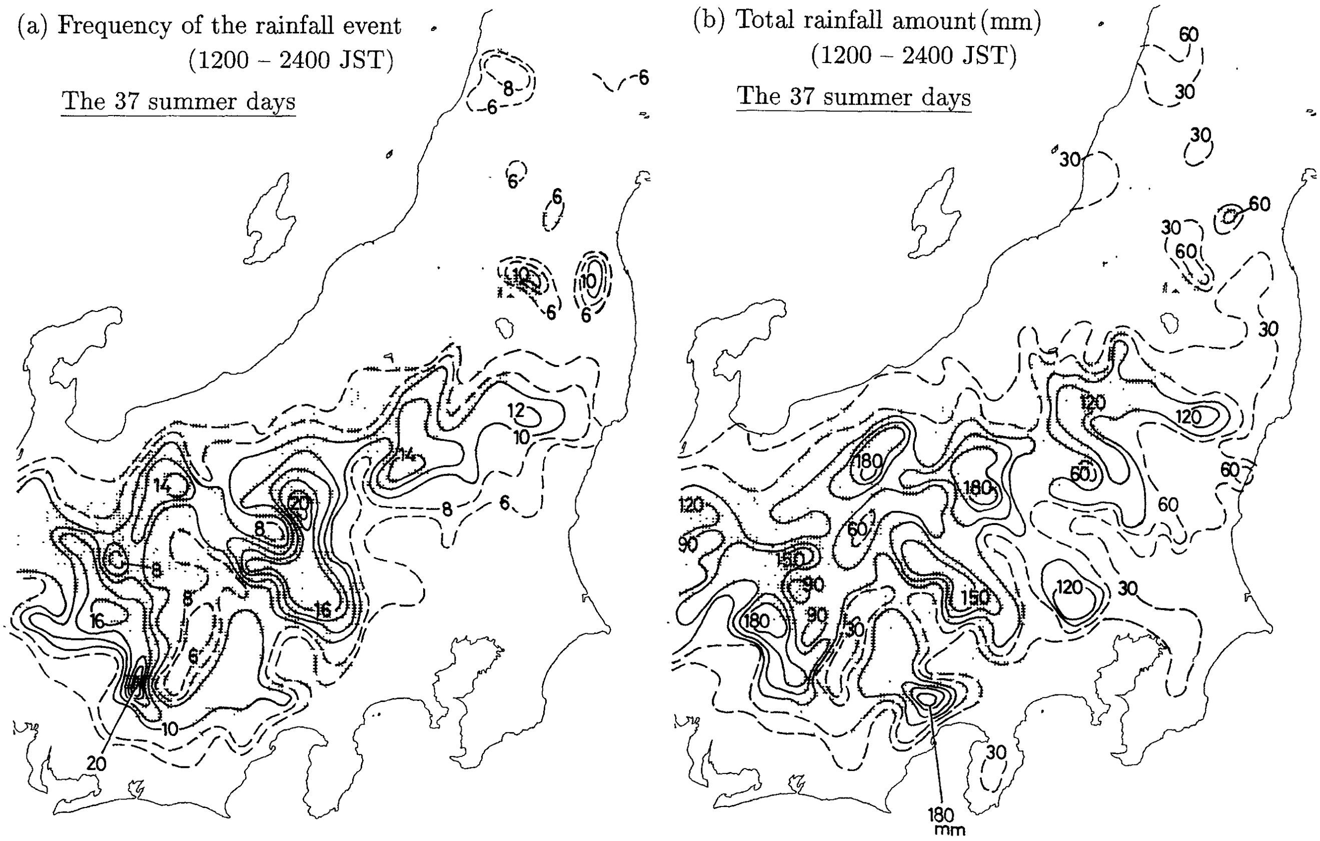

Fig. 5. (a) The frequency distribution of rainfall events that occurred from 1200 to 2400 JST for the 37 summer days. Only regions of the frequency greater than 6 are shown by contour lines. Regions of elevation higher than 800 m MSL, averaged over 10 km × 10 km grid boxes, are stippled. (b) The distribution of total rainfall amounts from 1200 to 2400 JST for the 37 days.

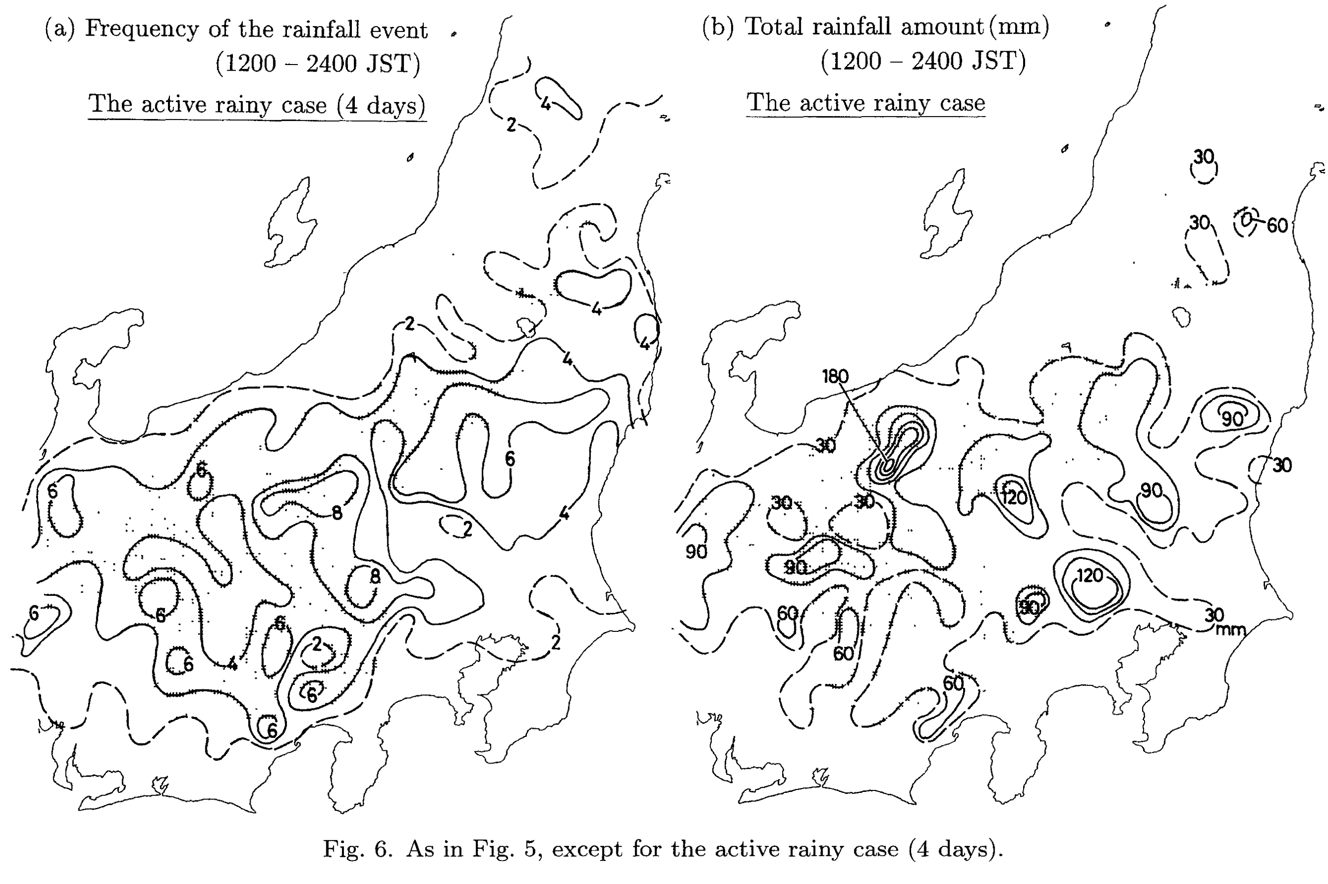

Fig. 6. As in Fig. 5, except for the active rainy case (4 days).

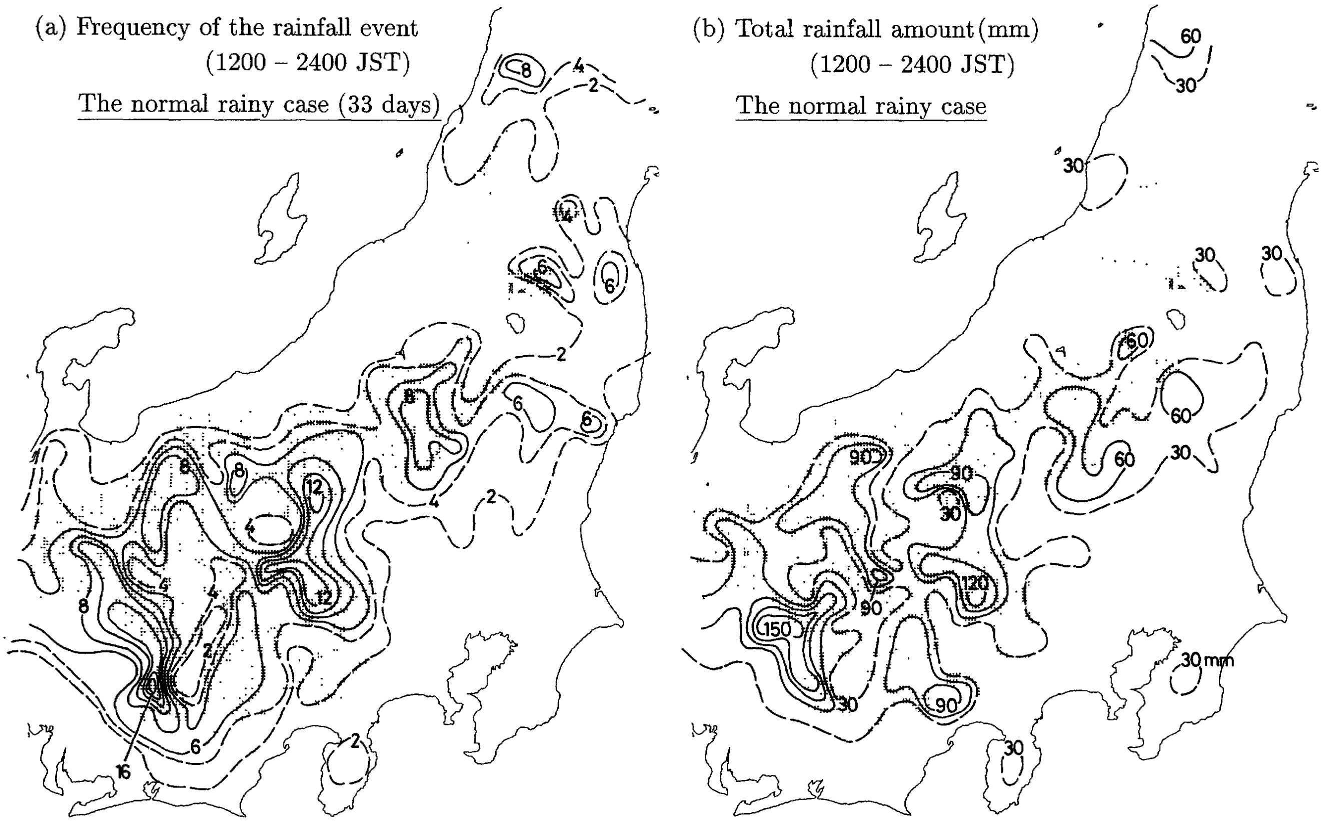

Fgi. 7. As in Fig. 5, except for the normal rainy case (33 days).

the normal rainy case. Although the rainfall events are concentrated in the mountainous regions for both the cases, the spatial concentration is weaker for the active rainy case. The frequency distribution of rainfall events for the normal rainy case is similar to that for the 37 summer days, except that the rain shower activity is not so great over the southeast side of mountains to the north of the Kanto Plain.

Furthermore, for the active rainy case, the consistency between the frequency of rainfall events and the total rainfall amount is not so good. In this case, a few severe rainfall events must have increased the total rainfall amount in some areas and were missed mainly due to lack of sampling data. This inconsistency for the active rainy case also affects the spatial distribution of the rainfall amounts for the 37 summer days (see Fig. 5b). On the other hand, the consistency between the frequency of rainfall events and the total rainfall amount is better for the normal rainy case. Figure 8 shows the quantitative relationship between the frequency of rainfall events and the total rainfall amount at each station from 1200 to 2400 JST (top panel: the active rainy case, bottom panel: the normal rainy case). The total rainfall amount is roughly proportional to the frequency of rainfall events only for the normal rainy case.

4. The relationship between the rain shower and the thermally induced local circulation

4.1 Thermally induced local circulation in the daytime

The characteristics of the surface wind and temperature fields over central Japan are investigated using the AMeDAS data. Figure 9 displays the 37-day mean wind and surface air temperature fields (a), and the frequency distributions of wind vector direction during the daytime (b) at 1500 JST. Here, the arrows indicate the wind vectors at a height of 100 m above the ground, calculated from the observed surface wind and the aerodynamic roughness length for each site (Kondo and Yamazawa, 1986; Kuwagata and Kondo, 1990), by assuming a logarithmic wind profile (see the Appendix A). The temperatures were reduced to mean sea level with the adiabatic lapse rate of $\Gamma_d = 0.00976$ K m^{-1}. These fields represent typical weather patterns for fair-summertime-weather conditions.

For fair-weather conditions during the summer, the wind field is characterized by a thermally induced local circulation over the heated land surface. That is, the wind vectors are directed inland, except over the interior inland basin, where the wind speed is rather weak. Although the wind field directed inland consists of both the sea breeze in the coastal areas and upslope-upvalley winds over the inland ar-

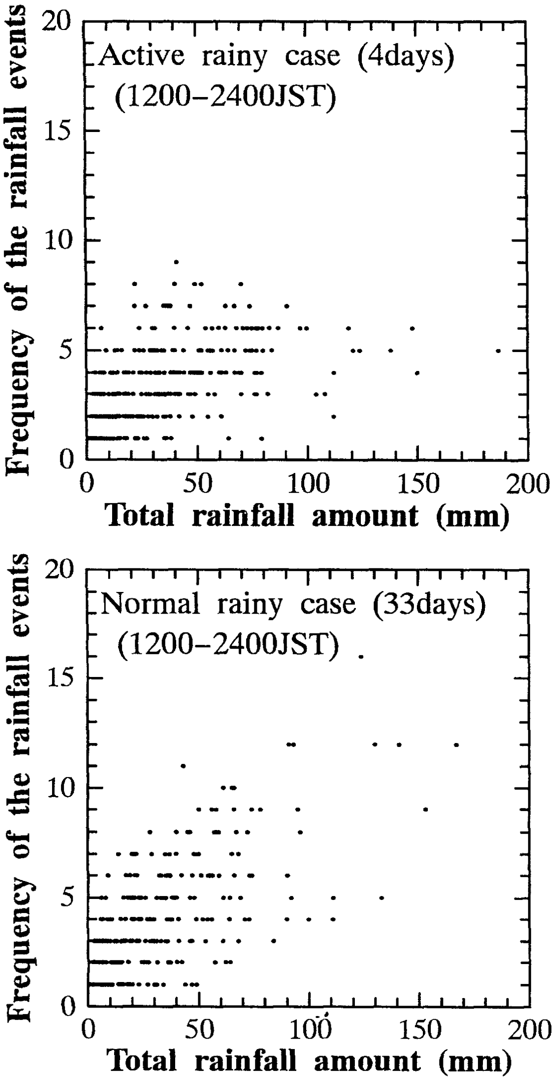

Fig. 8. The quantitative relationship between the frequency of rainfall events and the total rainfall amount at each station from 1200 to 2400 JST (top panel: the active rainy case, bottom panel: the normal rainy case).

eas, the boundaries of both circulations are not so clear. The upslope-upvalley winds are divided into several local wind systems by the mountain ranges. The afternoon temperature increases as the distance from the coastal areas increases, whereas the interior inland basin has nearly uniform temperatures. The statistical distributions of the wind vector direction frequency suggest that the wind directions at most sites are almost invariant from day to day. That is, the surface wind field patterns in central Japan are mostly invariant during the 37 summer days. The development of the thermally induced circulation is closely related to the thermal low forming over the inland area of central Japan during the daytime (Kurita *et al.*, 1985; 1990; Ueda *et al.*, 1988; Kimura and Kuwagata, 1993); the thermal low corresponding to the thermal contrast between the coastal and inland regions (Kuwagata and Sumioka, 1991).

Figure 10 shows the 46 days of spring mean wind and surface air temperature fields at 1500 JST, under fair-weather and weak synoptic wind conditions. These fields are almost the same as those for the 37 days of summer. The wind fields for each of the 46 days also exhibit similar patterns (not shown). The strength of the surface wind speed and the thermal contrast from coast to inland are greater for the 46 day spring period, since the daytime heating of the ground surface due to solar radiation is stronger in the spring season.

The daytime wind and temperature fields for both the summer 37-day and the spring 46-day periods represent typical patterns of a thermally induced local circulation during a warm season under fair-weather and weak synoptic wind conditions. The day to day patterns of these fields are almost invariant.

4.2 The role of the thermally induced local circulation in the development of rain showers

According to Section 3c, the rainfall events are concentrated over the mountainous regions, whereas the daytime thermally induced local circulation is also directed toward the mountainous regions. In order to clarify the mesoscale convergence of the circulation, horizontally band-pass-filtered surface wind data from the AMeDAS stations are used to calculate the horizontal mesoscale convergence. In this analysis, the original wind data were first interpolated to wind speeds at 100 m above the ground using the same procedure as in Fig. 9. The band-pass-filtered surface winds were then calculated with the use of the band-pass filter suggested by Doswell (1977, see the Appendix B). The parameters for the band-pass filter are same as those used in a similar analysis by Nakai (1983). The horizontal scale of the filter is 100 km, which corresponds to the scale of the daytime local circulation over central Japan.

Figure 11 shows the areas of convergence in central Japan at 1500 JST for the 37 summer days, calculated using such a procedure. It should be noted that unrealistic distributions of convergence are calculated in some areas due to lack of surface wind data. Figure 12 shows the illustration of the daytime surface wind field, inferred from the distributions of the AMeDAS surface winds (Fig. 9) and the horizontal convergence (Fig. 11). Here, the boundaries of each local wind system correspond to the convergence areas.

According to this result, the thermally induced local circulation displays a distinct convergence in the afternoon over the mountain ranges. Most of these mountainous regions also exhibit stronger activity of rain shower (see Figs. 5–7). There is no distinct convergence in the active rainy area spreading over

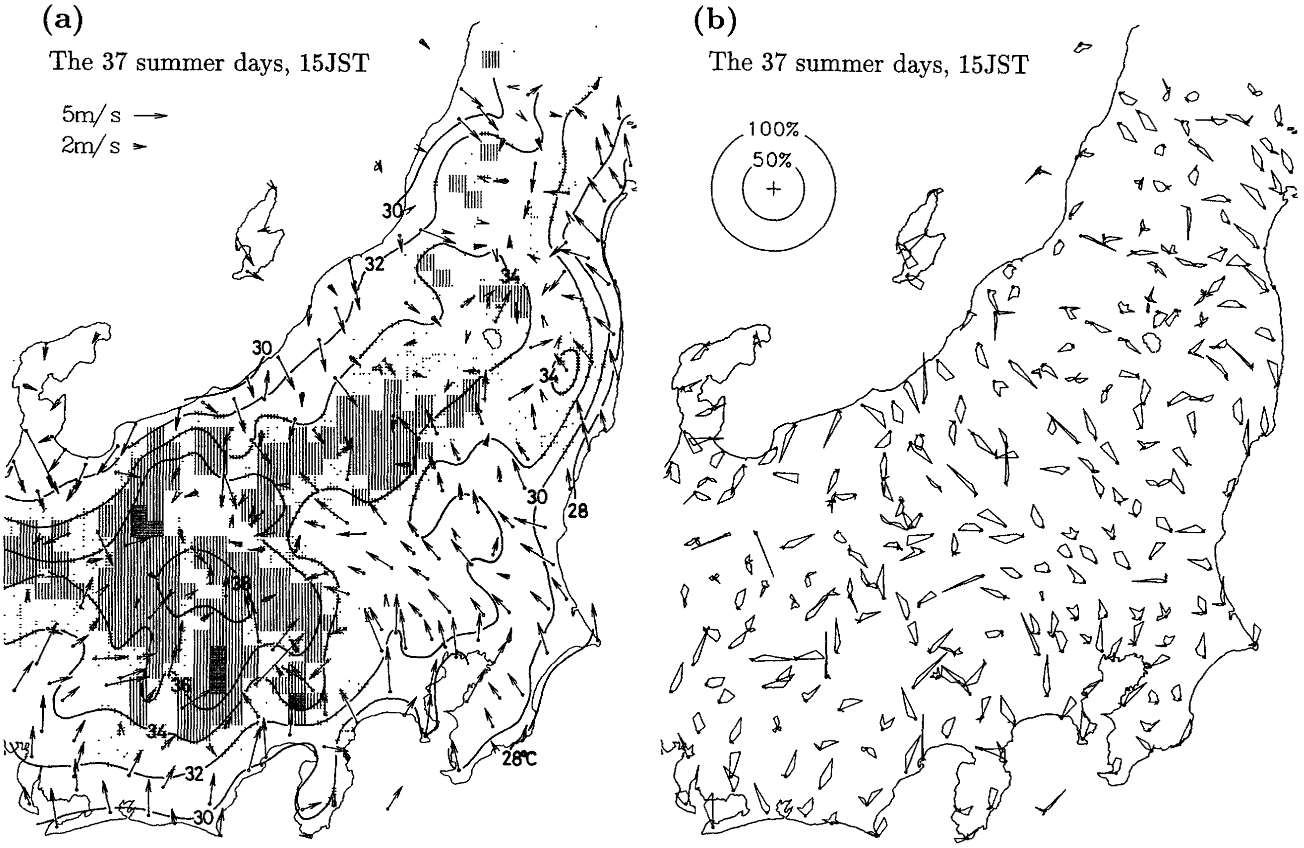

Fig. 9. (a) The wind and surface air temperature fields at 1500 JST averaged over the 37 summer days. Here, the arrows indicate the wind vectors at a height of 100 m above the ground (see the Appendix A), and the temperatures were reduced to mean sea level with the adiabatic lapse rate of $\Gamma_d = 0.00976$ K m^{-1}. The three degrees of stippling denote areas of elevation $z \geq 500, 1000, 2000$ m MSL, respectively (each elevation is averaged over 10 km × 10 km grid boxes). (b) The statistical distributions of the frequency of wind vector direction at 1500 JST for the 37 summer days. The length scales for representing the frequency of each wind vector direction are indicated by the double circles in the upper left of the figure.

the southeast side of mountains in the north of the Kanto Plain, which result can be explained by the movement of the active rainy area with time (refer the 1st and 2nd paragraphs in Section 3c). Although convergence areas due to the sea breeze front also exist over the Kanto Plain (indicated by the letters A and B in Fig. 12), greater frequencies of the rainfall events are found only in a small part of such areas for the active rainy case (see Fig. 6). On the other hand, somewhat stronger activity of rain shower can be found over convergence areas near the inlets of the Kofu Basin and the Ina Valley.

According to previous study, the daytime thermally induced local circulation contributes to increased water vapor content during the daytime over the mountainous regions where the circulation converges. That is, the thermally induced circulation over complex terrain transports water vapor from the plain and basin areas to the mountainous area, resulting in an accumulation of moist air over the mountainous region during the late afternoon (Kimura and Kuwagata, 1995). The greatest amounts of water vapor are accumulated over the mountainous region when the horizontal scale of the topography is close to 100 km, which is nearly the same as the horizontal scale of each mountain range, basin, and plain in central Japan.

Figure 13 displays the daily variations of specific humidity at the 3 meteorological stations averaged over the 37 summer days (top panel) and the 46 spring days (bottom panel). Here, *Tokyo* is located on the plain near the coast at an altitude of 5.3 m MSL, *Matsumoto* at the bottom of a basin in the inland area at an altitude of 610.0 m MSL, and *Nikko* in the mountainous area at an altitude of 1291.9 m MSL (see Fig. 12). For the afternoon of both periods of summer and spring, the values of specific humidity in the plain and in the basin exhibit minimum values around 1500 JST, while those in the mountainous area have maximum values, which probably result from the water vapor transport in the thermally induced local circulation. Furthermore, the specific humidity in the mountainous area is greater than that at the basin bottom around 1500 JST.

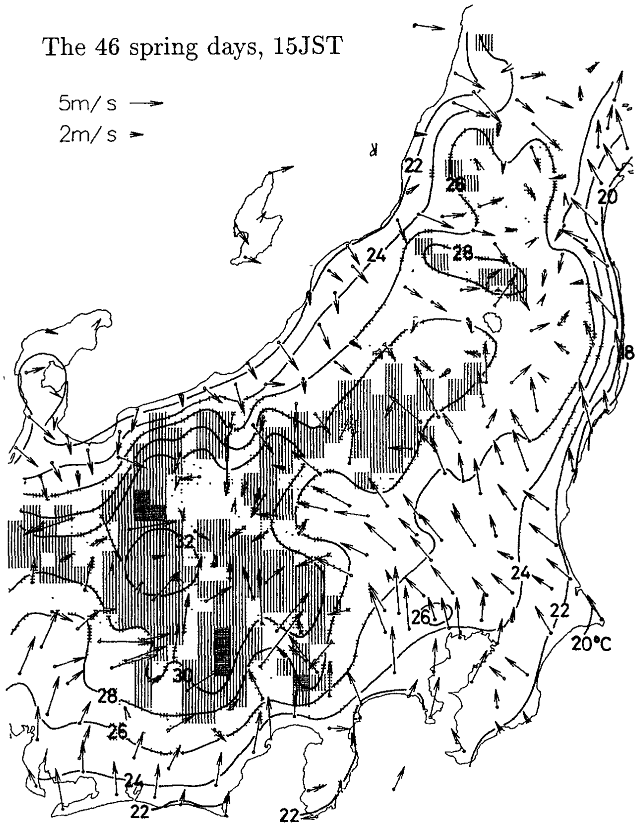

Fig. 10. The wind and surface air temperature fields at 1500 JST, averaged over the 46 spring days.

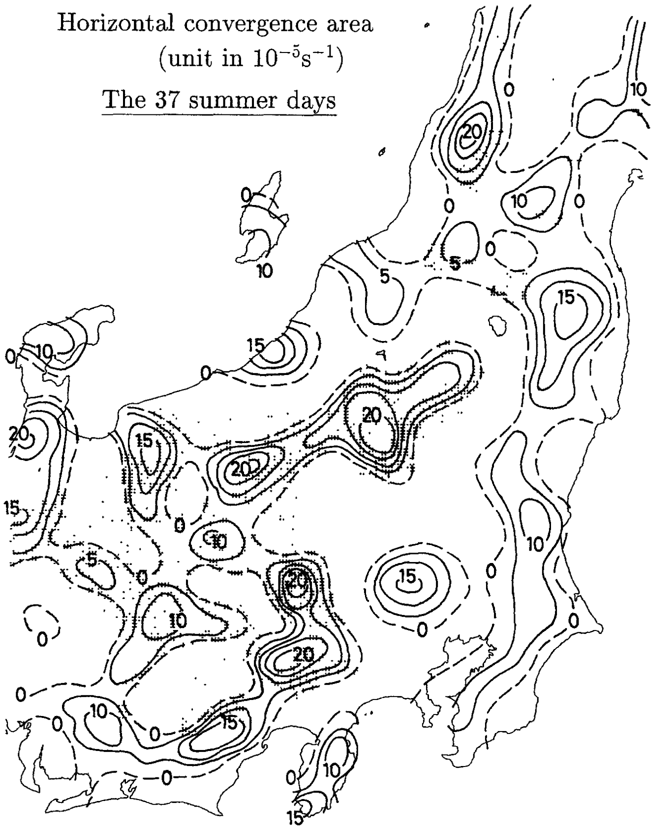

Fig. 11. The distribution of horizontal convergence at 1500 JST for the 37 summer days, calculated using band-pass filtered surface winds from the AMeDAS stations. The areas of convergence of the surface wind are indicated by contour lines having a $5 \times 10^{-5}s^{-1}$ interval. Regions of elevation (averaged over 10 km $\times$ 10 km grid boxes) higher than 800 m MSL are stippled.

The accumulated moist air over the mountainous region must contribute to the formation of cumulus clouds during the late afternoon. Figure 14 shows the spatial distributions of the sunshine duration from 1500 to 1600 JST averaged over the 37 summer days (a) and the 46 spring days (b), analyzed using the data from the 281 AMeDAS stations. For the 37 summer days, the sunshine duration decreases during the late afternoon over the mountainous regions, where the daytime rainfall events due to rain showers are concentrated (see Fig. 5). The sunshine duration is also somewhat lower in the convergence area of the sea breeze front in the Kanto Plain (indicated by the letter A in Fig. 12). According to previous studies, the sea breeze front in this region becomes intensified by the heat island effect of the Tokyo Metropolitan area (Kimura and Takahashi, 1991; Yoshikado, 1992). It can be expected that cumulus clouds formed in this region. Greater activity of the rain showers is also found in this region for the active rainy case (see Fig. 7).

The distribution of sunshine duration for the 46 days of spring is almost the same as that for the 37 days of summer. These results suggest that the thermally induced local circulation contributes to the formation of small-scale cumulus clouds over the mountainous region during the late afternoon, under fair weather and weak synoptic wind conditions from the spring to summer seasons. The afternoon rain showers occurred over the mountainous regions for the 37 summer days, whereas few rain showers occurred for the 46 spring days. This difference between spring and summer can be explained by the following hypothesis.

During the summer season, the small-scale cumulus clouds triggered by the thermally induced local circulation can develop into large-scale cumulus or cumulonimbus clouds under favorable conditions for developing moist convection, resulting in rain showers over the mountainous region in the late afternoon. On the other hand, the atmospheric precipitable water during the spring season is considerably less than that in summer (under 40 mm for all days), which is quite unfavorable for the development of moist convection . The small-scale cumulus clouds over the mountainous regions can not develop into large-scale cumulus clouds under such springtime conditions. That is, a rain shower can not be triggered by the thermally induced local circulation

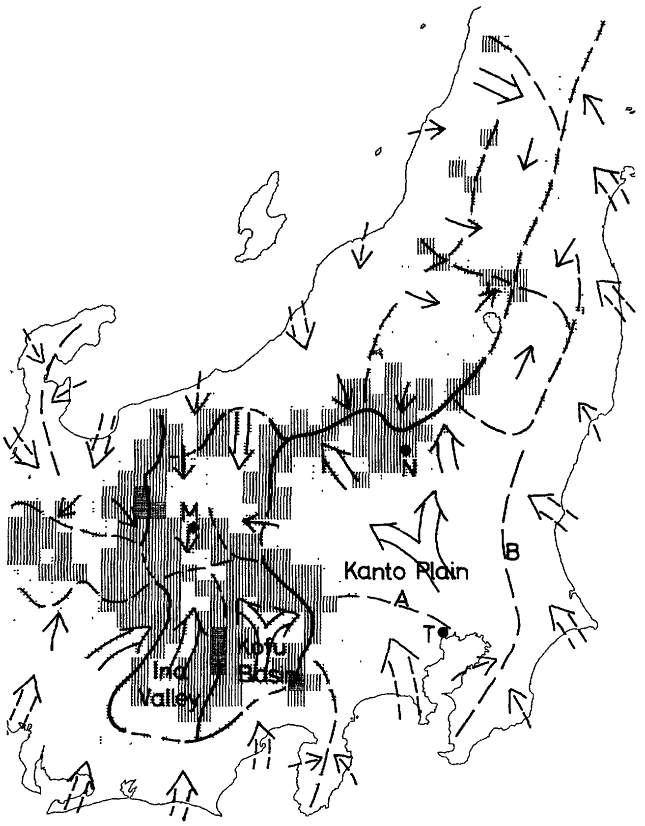

Fig. 12. Illustration of the daytime surface wind field, inferred from the distributions of the AMeDAS surface winds and the horizontal convergence. Clear boundaries of each local wind system are indicated by solid lines, and other boundaries by broken lines; letters A and B denote the sea breeze front in the Kanto Plain. The solid circles indicate the locations of 3 meteorological stations, T (Tokyo), M (Matsumoto), and N (Nikko), whose data are analyzed in Fig. 13. The locations of the Kanto Plain, Kofu Basin, and Ina Valley are also indicated.

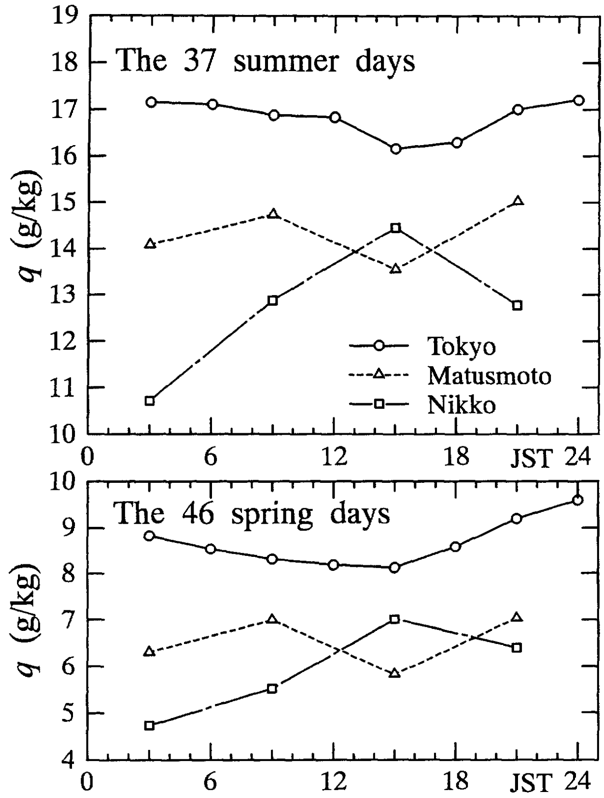

Fig. 13. The daily variations of specific humidity q at the 3 meteorological stations in Fig. 12 averaged over the 37 summer days and the 46 spring days. Here, *Tokyo* is located on the plain near the coast, *Matsumoto* at the bottom of a basin over the inland area, and *Nikko* in the mountainous area (see Fig. 12).

during the spring season.

It should be noted that the consistency between the areas where the afternoon sunshine duration decreased and the convergence areas of local winds is somewhat better than that between the areas having stronger activity of rain shower and the convergence areas. For example, although the afternoon sunshine duration decreased in the strong convergence area south of the Akaishi Mountains (the mountain range between the Kofu Basin and the Ina Valley), rain shower activity was not so great in this area. Further, in some mountainous areas, the area having strong rain shower activity spread in the side of the convergence area although the afternoon sunshine duration decreased just over the convergence area. The reason why this difference was evident is not clear at the present time.

Figure 15 illustrates the visible images from the GMS at 1500 JST for 3 cases (2, 17, and 18 August 1985) of the 37 summer days. In all cases, cumulus clouds have developed over the mountainous regions. These satellite images are consistent with the statistical results (Figs. 5–7 and 14) obtained using precipitation and sunshine duration data from the surface meteorological network.

5. Summary

The summer rain showers which developed in central Japan under otherwise fair-weather conditions during the summer of 1985 were investigated using routine observational data from weather stations in order to examine both the characteristics of summer rain shower and the contribution of the thermally induced local circulation to the development of rain showers. The results can be summarized as follows:

1) According to the statistical analysis of 37 days of sunny summer weather, the diurnal cycle of precipitation exhibited a distinct peak in rainfall around 1800 JST, while there was little rainfall from 0000 to 1200 JST. The distinct afternoon

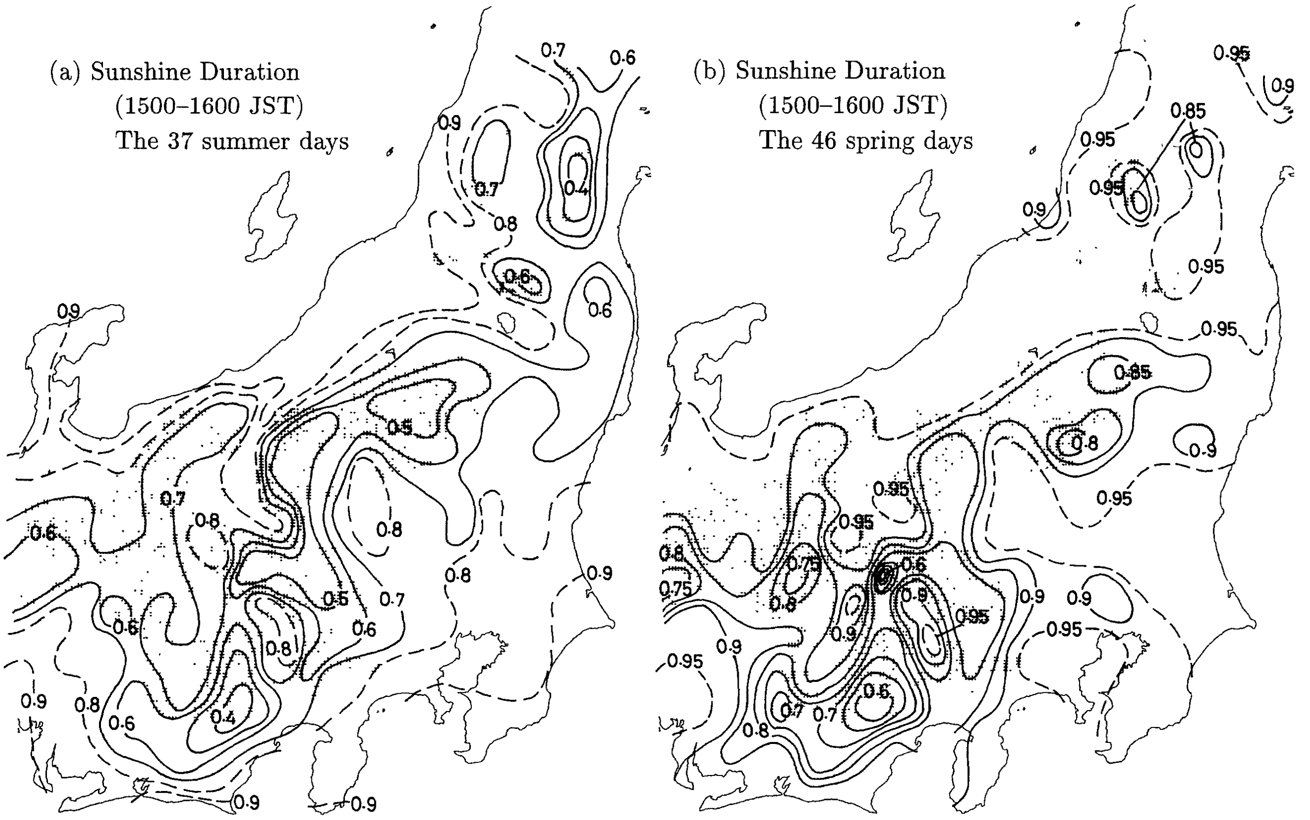

Fig. 14. The spatial distributions of the sunshine duration from 1500 to 1600 JST, averaged for the 37 summer days (a), and the 46 spring days (b), analyzed using the data from the 281 AMeDAS stations. The sunshine duration is shown by the value of N/N_0, where N (min) is the sunshine duration from 1500 to 1600 JST averaged for each period, and $N_0 = 60$ min. The regions of elevation (averaged over 10 km $\times$ 10 km grid boxes) higher than 800 m MSL are stippled.

peak was caused by rain showers. Rain shower activity increased as the atmospheric static stability for dry (or moist) convection decreased under conditions that the atmospheric precipitable water exceeded 40 mm. Rain showers were concentrated in the mountainous regions, and the areas where rain showers were concentrated largely did not move with time. The spatial concentration of the rain showers however was lower when rain showers were more active.

2) On the other hand, a thermally induced local circulation developed over central Japan during the daytime under sunny conditions from the spring to summer seasons, due to the thermal forcing from the heated ground surface. The surface wind field was directed inland, having a strong dependence on topography, and converged over the mountainous regions. Most of these mountainous regions exhibited stronger rain shower activity for the 37 summer days.

3)Water vapor pressure measured in the mountainous area displayed a maximum value in the afternoon under sunny conditions from the spring to summer. This result is consistent with the previous study which suggested that the thermally induced local circulation contributes to an increase in the water vapor content over the mountainous regions during the daytime. According to the previous study, the greatest amounts of water vapor are accumulated over the mountainous region in the late afternoon when the horizontal topographic scale is close to 100 km, which is nearly the same as the horizontal scale of each mountain range, basin, and plain in central Japan. The accumulated moist air over the mountainous regions is favorable for the development of small-scale cumulus clouds, and the formation of clouds was confirmed by the horizontal distribution of sunshine duration measured at the AMeDAS stations in the late afternoon. Finally, it can be expected that the small-scale cumulus clouds develop into large-scale cumulus or cumulonimbus clouds under favorable conditions for the development of moist convection in the summer, causing the rain showers over mountainous regions during the late afternoon.

These results were derived from a statistical analysis for the 37 sunny summer days in 1985. In order to further clarify the general characteristics of the summer rain shower in central Japan, it is desirable to make similar and another kinds of analy-

2 August 1985 (1500 JST)

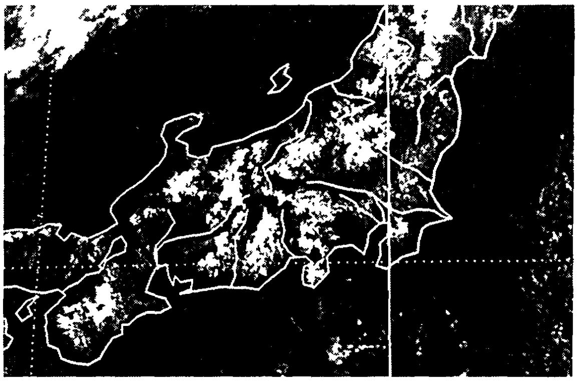

17 August 1985 (1500 JST)

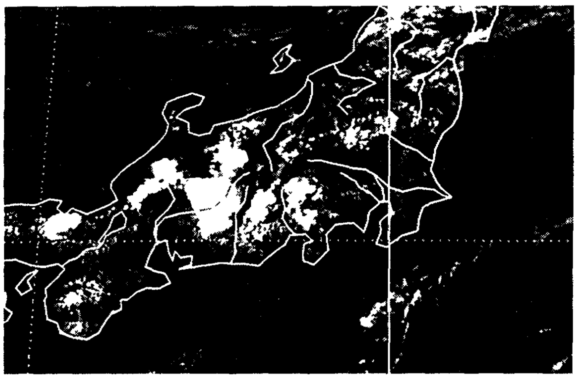

18 August 1985 (1500 JST)

Fig. 15. Visible images from the GMS at 1500 JST for 3 cases (2, 17, and 18 August 1985) of the 37 summer days.

ses for the summer seasons over several years. On the other hand, the analysis of some rain shower events is also useful to investigate the influence of the upper-level synoptic wind on the movement of rain shower clouds. Since the present study has shown the possibility that rain showers are triggered by the thermally induced circulation, further studies will be necessary to examine the mechanism of the development of rain shower cloud.

Acknowledgments

The author would like to thank Prof. J. Kondo of Tohoku University, Prof. F. Kimura of Tsukuba University, and Dr. H. Kanno of the Tohoku National Experiment Station for helpful discussions and useful advice. Thanks are also extended to Mr. S. Akashi of the Meteorological Satellite Center of the JMA for providing the GMS data. The routine observational data at the meteorological stations were provided by the JMA. The two-dimensional graph-plot tool, developed by Dr. K. Edamatsu of Tohoku University, was used in the drawing of the figures.

Appendix

A. Calculation of 100-m wind speeds

Wind speeds at 100 m above the ground were calculated for each AMeDAS station with the use of

$$V_{100\ \mathrm{m}} = V_{obs}\frac{\ln(z_r/z_0)}{\ln(z/z_0)}, \tag{A1}$$

where $V_{100\ \mathrm{m}}$ is the wind speed at 100 m, V_{obs} the observed wind speed, z the height of the wind vane above the ground, z_0 the aerodynamic roughness length, and $z_r = 100$ m.

B. The band-pass filter for calculating the horizontal mesoscale convergence

The band-pass filtered surface winds were calculated from the wind data at the AMeDAS stations, in order to calculate the horizontal mesoscale convergence. The spatial filtering technique suggested by Doswell (1977) was used in the present study. The filtering procedure is described below.

First, the analysis area is divided into a mesh having 10 km $\times$ 10 km square grid boxes. The wind vector is interpolated to each grid box using the wind data at the AMeDAS stations.

$$\vec{V}^{(a)} = \sum_{m=1}^{M} w_a\vec{V}_m / \sum_{m=1}^{M} w_a, \tag{A2}$$

and

$$\vec{V}^{(b)} = \sum_{m=1}^{M} w_b\vec{V}_m / \sum_{m=1}^{M} w_b, \tag{A3}$$

where $\vec{V}^{(a)}$ and $\vec{V}^{(b)}$ are the interpolated wind vectors for each grid box using the weighting functions w_a and w_b, $\vec{V}_m$ $(m = 1, 2, \cdots)$ is the wind vector at 100 m above the ground at the AMeDAS station located within 80 km $(=R_c^*)$ of a given grid box (see the Appendix A), and M the number of corresponding AMeDAS stations, respectively. The weighting functions are given by

$$w_a = \exp[-(\rho^2 R^2)/(4D_a^2)], \tag{A4}$$
$$w_b = \exp[-(\rho^2 R^2)/(4D_b^2)], \tag{A5}$$

where

$$R = R^*/(\rho \Delta S). \tag{A6}$$

Here, R^* is the distance between a given grid box and each AMeDAS station, R the non-dimensional value of R^*, ΔS (= 10 km) the spatial grid interval, and ρ the non-dimensional constant, respectively. The value of $\rho \Delta S$ represents the characteristics length scale of R^*, and $\rho = 2$ was assumed here. Further, D_a^2 and D_b^2 are the non-dimensional parameters related to the characteristics of the weighting functions.

The parameters D_a^2 and D_b^2 must hold the following equations.

$$D_a^2 = 2\ln(k_1/k_2)\ \pi^{-2}(k_1^2 - k_2^2)^{-1}, \tag{A7}$$

$$D_b^2 = 2\ln(k_2/k_3)\ \pi^{-2}(k_2^2 - k_3^2)^{-1}, \tag{A8}$$

and

$$k_1 = (\pi D_a)^{-1}\{-\ln[\exp(-\pi^2 D_a^2 k_2^2) + \exp(-\pi^2 D_b^2 k_2^2) - \exp(-\pi^2 D_b^2 k_3^2)]\}^{1/2}. \tag{A9}$$

Here, the non-dimensional wavenumbers k_i ($i = 1 \sim 3$) related to the characteristics of the band-pass filter are given by

$$k_i = 2\Delta S/L_i^*, \tag{A10}$$

where L_i^* ($i = 1 \sim 3$) are the characteristic length scales for spatial filtering. Having chosen k_2 and k_3, Eqs. (A7)$\sim$(A9) can be solved for D_a^2, D_b^2 and k_1.

The interpolated wind vectors $\vec{V}^{(a)}$ and $\vec{V}^{(b)}$ in Eqs. (A2) and (A3) represent the low-passed filtered winds which have the non-dimensional cutoff wavenumbers k_1 and k_3, respectively. The band-pass filter in the present study has a peak response at the non-dimensional wavenumber $k = k_2$. Finally, the band-pass filtered wind vector $\vec{V}^{(b-a)}$ for each grid box is evaluated by

$$\vec{V}^{(b-a)} = (\vec{V}^{(b)} - \vec{V}^{(a)})/\delta r, \tag{A11}$$

where

$$\delta r = \exp(-\pi^2 D_b^2 k_2^2) - \exp(-\pi^2 D_a^2 k_2^2). \tag{A12}$$

The parameters used in the present study are $k_1 = 0.1143$, $k_2 = 0.2$, $k_3 = 0.35$, $D_a = 2.0518$, and $D_b = 1.1725$. The band-pass filter in the present study has a peak response at a spatial wavelength of 100 km.

References

Doswell III, C.A., 1977: Obtaining meteorologically significant surface divergence fields through the filtering property of objective analysis. *Mon. Wea. Rev.*, **105**, 885–892.

Fujibe, F., 1988: Diurnal variation of precipitation and thunderstorm frequency in Japan in the warm season. *Pap. Meteor. Geophys.*, **21**, 79–94.

Kimura, F., 1994: Horizontal transport of moisture by local circulation. *Tenki*, **41**, 313-320 (in Japanese).

Kimura, F. and T. Kuwagata, 1993: Thermally induced wind passing from plain to basin over a mountain range. *J. Appl. Meteor.*, **32**, 1538–1547.

Kimura, F. and T. Kuwagata, 1995: Horizontal heat fluxes over a complex terrain computed using a simple mixed-layer model and a numerical model. *J. Appl. Meteor.*, **34**, 549–558.

Kimura, F. and S. Takahashi, 1991: The effects of land-use and anthropogenic heating on the surface temperature in the Tokyo Metropolitan area: A numerical experiment. *Atmos. Environ.*, **25B**, 155–164.

Kondo, J. and H. Yamazawa, 1986: Aerodynamic roughness over an inhomogeneous ground surface. *Boundary-Layer Meteor.*, **35**, 331–348.

Kurita, H., K. Sasaki, H. Muroga, H. Ueda and S. Wakamatsu, 1985: Long-Range transport of air pollution under light gradient wind conditions. *J. Climate Appl. Meteor.*, **24**, 425–434.

Kurita, H., H. Ueda and S. Mitusmoto, 1990: Combination of local wind systems under light gradient wind conditions and its contribution to the long-range transport of air pollutants. *J. Appl. Meteor.*, **29**, 331–348.

Kuwagata, T. and F. Kimura, 1995: Daytime boundary layer evolution in a deep valley. Part I: Observations in the Ina Valley. *J. Appl. Meteor.*, **34**, 1082–1091.

Kuwagata, T. and F. Kimura, 1997: Daytime boundary layer evolution in a deep valley. Part II: Numerical simulation of the cross-valley circulation. *J. Appl. Meteor.*, **36**, (in press).

Kuwagata, T. and J. Kondo, 1990: Estimation of aerodynamic roughness at the regional meteorological stations (AMeDAS) in the central part of Japan. *Tenki*, **37**, 55–59 (in Japanese).

Kuwagata, T. and M. Sumioka, 1991: The daytime PBL heating process over complex terrain in central Japan under fair and calm weather conditions :Part III, Daytime thermal low and nocturnal thermal high. *J. Meteor. Soc. Japan*, **69**, 91–104.

Kuwagata, T., M. Sumioka, N. Masuko and J. Kondo, 1990: The daytime PBL heating process over complex terrain in central Japan under fair and calm weather conditions :Part I Meso-scale circulation and the PBL heating rate. *J. Meteor. Soc. Japan*, **68**, 625–638.

Nakai, K., 1983: An analysis of surface divergence field through the band-pass filter — Thunderstorms of 11 August 1979 in the Kanto region —. *J. Meteor. Res.*, **35**, 109–118 (in Japanese).

Oki, T. and K. Musiake, 1994: Seasonal change of the diurnal cycle of precipitation over Japan and Malaysia. *J. Appl. Meteor.*, **33**, 1445–1463.

Shimizu, S., 1964: On the diurnal variation of the winds accompanied by thermal high or low in the central region of Japan. *Tenki*, **11**, 138–141 (in Japanese).

Suzuki, R., 1991: The influence of daytime heating and nocturnal cooling on the surface airflow patterns over central Japan. *Inter. J. Climatol.*, **11**, 297–313.

Tatehira, R. and M. Hoshina, 1993: Regional variation in diurnal change of heavy rainfall. *Tenki*, **40**, 325–333 (in Japanese).

Udagawa, K., 1966: Relationship between heat low and thunderstorm. *J. Meteor. Res.,* **18**, 487–489 (in Japanese).
Udagawa, K., 1968: Relationship between heat low and thunderstorm (2nd Report). *J. Meteor. Res.,* **20,** 657–665 (in Japanese).
Ueda, H., S. Mitusmoto and H. Kurita, 1988: Flow mechanism for the long-range transport of air pollutants by the sea breeze causing inland nighttime high oxidants. *J. Appl. Meteor.,* **27**, 182–187.
Yoshikado, H., 1992: Numerical study of the daytime urban effect and its interaction with the sea breeze. *J. Appl. Meteor.,* **31**, 1146–1164.

中部日本域における夏季の短時間降雨に関する解析およびその熱的局地循環との関連性

桑形恒男
（農林水産省東北農業試験場）

1985年夏季の晴天条件下に中部日本域で発生した短時間降雨を、ルーチン気象観測データを用いて統計的に解析した。解析期間の中部日本域における降水量は夕方の18時ぐらいに顕著なピークを持ち、0時から12時までの深夜から午前中にかけての時間帯にはほとんど降水がなかった。夕方の顕著な降水ピークは、午後になって発生する驟雨性の短時間降雨に対応したものである。日々のデータについて見ると、このような降雨は可降水量40 mm以上の気象条件下で発生しやすくなり、その活動度は乾燥(または湿潤)対流に対する大気安定度の減少にともなって増加していた。短時間降雨の降雨域は内陸の山岳地帯に集中しており、降雨頻度が高い地域の時間による移動はあまり大きくなかった。ただし降雨域の山岳への集中の程度は，短時間降雨の活動が活発な日ほど小さくなる傾向があった。

一方、中部日本域では春季から夏季にかけての一般風が弱い晴天日の日中に、連日のように熱的な局地循環が発達する。熱的局地循環は地形の影響を強く受けており、内陸の山岳が局地循環の顕著な収束域となっていた。以前に実施された研究によって、熱的局地循環が平野および盆地(盆地底)から山岳に水蒸気を輸送する働きを持つことと、中部日本域のような100 km程度の水平スケールを持つ地形で、夕方における山岳上での水蒸気の蓄積が最大となることが明らかになっている。すなわち内陸の山岳では水蒸気の蓄積によって午後になると積雲が生成しやすくなり、今回の地上気象データの解析からも、午後の山岳域における水蒸気量の増加と日照率の低下が認められた。実際の短時間降雨にともなった降雨域もこのような山岳域に集中しいることから、熱的局地循環の発達が夏季の中部日本における対流性降雨の発生のトリガーとなっている可能性が本解析により示唆されたといえる。